AdLeaf: Quantitative leaf reconstruction from TLS point clouds

Guangpeng Fan, Liangliang Xu, Jiani Guo, Ruoyoulan Wang, Haoran Zhao, Hao Lu, Jinhu Wang, Di Wang, Feixiang Chen, Liangliang Nan

***Abstract*—Quantitatively reconstructing the 3D structure of individual leaves within tree canopies is critical for understanding forest function and environmental responses to climate change. While quantitative structure models (QSMs) using terrestrial laser scanning (TLS) effectively capture woody structures, they lack the capability to accurately reconstruct non-woody leaf components. This study proposes AdLeaf (Accurate and Detailed Leaf), a novel approach for fine-scale reconstruction of individual leaves using TLS point clouds. AdLeaf combines wood-leaf separation, individual leaf segmentation, detection and repair of incomplete leaves, explicit reconstruction, and parameter extraction. It automates semantic segmentation at the tree scale to separate woody and leafy components. Instance segmentation is refined through similarity graphs. Incomplete leaves are detected and repaired using shape concavity analysis and symmetry-based mirroring. AdLeaf enables direct measurement of leaf attributes, including count, area, inclination, volume, and azimuth.**

Validation using field scans, synthetic data, and both in-situ and destructive measurements shows high accuracy: leaf counting errors ranged from 0.58% to 8.23% for trees with 201-4,000 leaves. Reconstructed leaf geometries had mean and standard deviations below 0.83 cm and 0.70 cm, respectively. Leaf area measurements (10–180 cm^2) achieved a coefficient of determination (R^2) of 0.95, bias of -0.20 cm^2, and root mean square error of 5.63 cm^2. Incomplete leaf detection errors were below 28%, with the repaired area relative RMSE reduced by 9.4%. By addressing QSM limitations, AdLeaf enables explicit 3D leaf reconstructions that support detailed analysis of canopy light interception, spatial heterogeneity, and photosynthesis. It provides a robust framework for linking leaf structure to function at the tree level, advancing forest structure and radiative transfer research.

***Index Terms*—Terrestrial laser scanning, Quantitative reconstruction of non-woody parts, Physical structure, QSM, Tree-level individual leaf measurement**

I. Introduction

TREE structure, encompassing the 3D arrangement of stems, branches, and leaves, plays a crucial role in photosynthesis and tree function. The spatial distribution and shape of leaves determine a tree's ability to efficiently intercept and distribute light. While radiative transfer models simulate light distribution, accurately representing individual leaves at the tree scale remains a challenge [1], [2]. Many models simplify canopies into aggregated entities or stratified layers, using virtual leaves that fail to capture spatial heterogeneity, which introduces uncertainties in remote sensing applications [3]. Precise estimation of leaf structural traits is essential for predicting tree functions, such as respiration and biomass, and for understanding tree adaptation to environmental changes [4]–[6]. The growing demand for forest monitoring highlights the need for advanced methods to extract tree structural features. LiDAR technology (Light Detection And Ranging), particularly terrestrial laser scanning (TLS), offers non-destructive, high-precision 3D measurements ideal for near-field forest sensing [7]–[9]. TLS excels at creating detailed 3D representations of trees, making it a powerful tool for extracting tree structural features [10], [11]. This study uses TLS to reconstruct individual leaves within tree canopies and extract their structural parameters.

Traditional methods for quantifying leaf traits rely on manual measurements, which are time-consuming, labor-intensive, and often destructive, hindering result replication and failing to capture the spatial distribution and topological relationships of leaves within the canopy [12]–[14]. While photogrammetry has been applied to low-lying plants, its extension to tall woody species remains challenging [15], [16]. Advances in computational power have popularized 3D reconstruction techniques for tree structural traits [17], [18], but achieving high geometric accuracy remains a significant challenge. Precise measurements are essential for remote sensing and ecological modeling [19]. Optical remote sensing provides high-resolution multispectral data for stand- or regional-scale analyses [20] but lacks the resolution needed for tree- or leaf-scale structures. Some studies have utilized TLS point clouds to infer leaf positions and reconstruct trees at the leaf scale, but often aggregate point clouds to approximate canopy shapes [21]–[23]. In sparse vegetation or leaf-off periods, "branch skeleton" models estimate leaf positions, though their universal applicability remains uncertain [24]–[26]. Despite advancements, current methods face significant limitations in quantitatively reconstructing individual leaves.

Some 3D tree reconstruction models may appear visually credible, but their accuracy for quantitative remote sensing applications, such as radiative transfer, remains uncertain [27], [28]. Côté et al. emphasized that reconstructed models must replicate the radiative transfer properties of real plants. This requirement was validated in pine species [29], [30]. Similarly, Ollinger identified key factors influencing near-infrared (NIR) canopy reflectance, such as leaf angle distribution, aggregation, and optical properties [31]. However, the complex canopy structure complicates understanding these factors' relative contributions. Ollinger further demonstrated that traditional metrics like leaf area index (LAI) and canopy height are

Guangpeng Fan (fgp1994@bjfu.edu.cn), Liangliang Xu (xuliangliang@bjfu.edu.cn), Jiani Guo (JianiGuo905@bjfu.edu.cn), Ruoyoulan Wang (rylwang528@bjfu.edu.cn), Haoran Zhao (haoran01@bjfu.edu.cn), Hao Lu (luhao@bjfu.edu.cn), and Feixiang Chen (bjfxchen@bjfu.edu.cn) are with the School of Information Science and Technology, Beijing Forestry University, China.

Jinhu Wang (j.wang7@uva.nl) is with the Institute for Biodiversity and Ecosystem Dynamics, University of Amsterdam, Netherlands.

Di Wang (diwang@mail.xjtu.edu.cn) is with the School of Software Engineering, Xi'an Jiaotong University, China.

Liangliang Nan (liangliang.nan@tudelft.nl) is with the Urban Data Science Section, Delft University of Technology, Netherlands.

insufficient to fully explain canopy reflectance [32]. A comprehensive understanding of photon radiative transfer within the canopy requires considering tree spatial distribution, crown shape, and the arrangement and orientation of leaves [33], [34]. While leaf optical properties such as transmittance can be measured directly with spectrometers, quantifying leaf density, angle distribution, and spatial arrangement remains a significant challenge.

Recent advances in point cloud processing have enabled fine-scale estimation of structural traits in broadleaf forests [35], [36]. Voxel-based methods encode detailed information on leaf and woody densities, aggregation, angle distribution, and optical properties. Voxelized data can be integrated into radiative transfer models through ray tracing techniques to simulate canopy reflectance and absorption, providing insights into the factors affecting canopy reflectance [37]. However, many approaches estimate leaf distribution by proximity to branches, rather than directly mapping, which introduces deviations from actual canopy structures [38], [39].

Despite these advancements, achieving individual leaf-scale resolution remains a significant challenge [40]–[42]. QSM often fails to capture interior canopy leaf features [43], [44] due to its reliance on virtual leaves, limiting accurate representation of leaf angle distributions. While leaf normal estimation algorithms show potential, they often lack consistency in natural field conditions [45]. Methods such as planar fitting to estimate leaf normals, while effective for whole-tree analysis, remain labor-intensive [46]. Indirect methods, such as those using sunlight attenuation, offer integrated information but are limited in precisely locating leaf positions and shapes [47], [48].

TLS research primarily focuses on indirect estimation of leaf parameters, including Leaf Area Index (LAI), leaf inclination angles, and Leaf Angle Distribution (LAD). However, a universal method for directly measuring multiple leaf parameters within a quantitative reconstruction framework is still lacking. Existing TLS-based methods for estimating leaf area and related parameters can be classified into five categories: (1) Inversion methods, which use echo counts or intensity to estimate canopy gap fractions, are affected by distance, angle, and reflectance [49]; (2) Leaf plane fitting, which segments leaf clusters and fits planes to compute leaf normals [9], [45], is computationally complex and not scalable for multi-tree environments; (3) Voxel-based methods, which calculate contact frequencies to estimate leaf area density [35], [46], require uniform tree scanning; (4) Normal vector reconstruction, which identifies neighboring points to reconstruct leaf normals, though sensitive to noise and inconsistencies [9], [45]; and (5) Triangulation-based methods, which use point triplets to compute normal vectors [50], are vulnerable to noise and inaccuracies. Each category has its own limitations, and a unified framework balancing accuracy and scalability remains a challenge.

TLS now enables precise observation of individual tree leaves, allowing researchers to address long-standing QSM limitations in leaf reconstruction. A critical prerequisite for tree reconstruction from TLS point clouds is the separation of photosynthetic components (leaves) from non-photosynthetic components (branches and trunks), a process that relies on geometric and radiative features. Non-photosynthetic points typically exhibit higher density than photosynthetic ones due to factors like discrete leaf orientations, canopy gaps, and mutual occlusion. Methods such as Ferrara's use of density features with the DBSCAN algorithm and Tao's circle detection on horizontal slices have been employed to distinguish these components in broadleaf evergreen trees [51], [52]. Existing tools like CSF, Treeseg, and Lewos facilitate point cloud segmentation for separating ground, trees, branches, and leaves. This study builds on these techniques by refining leaf-level point cloud processing to extract detailed photosynthetic component features at the individual tree scale. Despite progress, most current methods remain visualization-focused [53], often relying on randomly placed generic leaf models that lack quantitative leaf traits [41], [54]. Limitations such as tree size, leaf distribution, sensor performance, point cloud processing workflows, and leaf occlusion continue to hinder TLS's full potential in leaf-scale studies [50], [55], [56]. This is a critical juncture for utilizing TLS to map complete canopy structures. Such advancements will improve the granularity of forest TLS point cloud analyses and enhance its contributions to high-resolution studies of forest ecological structure and function [22], [57].

Fig 1 illustrates the proposed AdLeaf method, which addresses the limitations of current state-of-the-art TLS point clouds processing approaches in quantitatively reconstructing individual leaves. AdLeaf achieves this by explicitly and accurately reconstructing individual leaves within the canopy, enabling the extraction of a comprehensive set of structural parameters, including leaf count, shape, size, surface area, volume, inclination, orientation, and position. Building on our previously published QSM framework [58], we systematically provide a TLS-based methodology for measuring the structure of branches and leaves at the tree scale [59]. We have developed a software prototype of the AdLeaf modeling workflow and plan to make it publicly accessible. The remote sensing data generated by AdLeaf, which describes the structural properties of plant canopies, holds the potential to supply detailed geometric and structural parameters for large-scale, high-resolution plant functional models at the leaf level [60]. The contributions of this paper are as follows:

- Propose a theoretical framework and methodology for measuring the photosynthetic components of trees, addressing QSM limitations in quantitative leaf reconstruction.
- Address canopy heterogeneity by quantifying the spatial and functional traits of individual leaves at the tree level.
- Provide a reliable tool for accurate leaf reconstruction, enabling studies of canopy light interception, resource allocation, and 3D radiative transfer.

II. Data Collection

We used TLS to collect detailed leaf data from real trees as well as synthetic simulations from virtual trees.

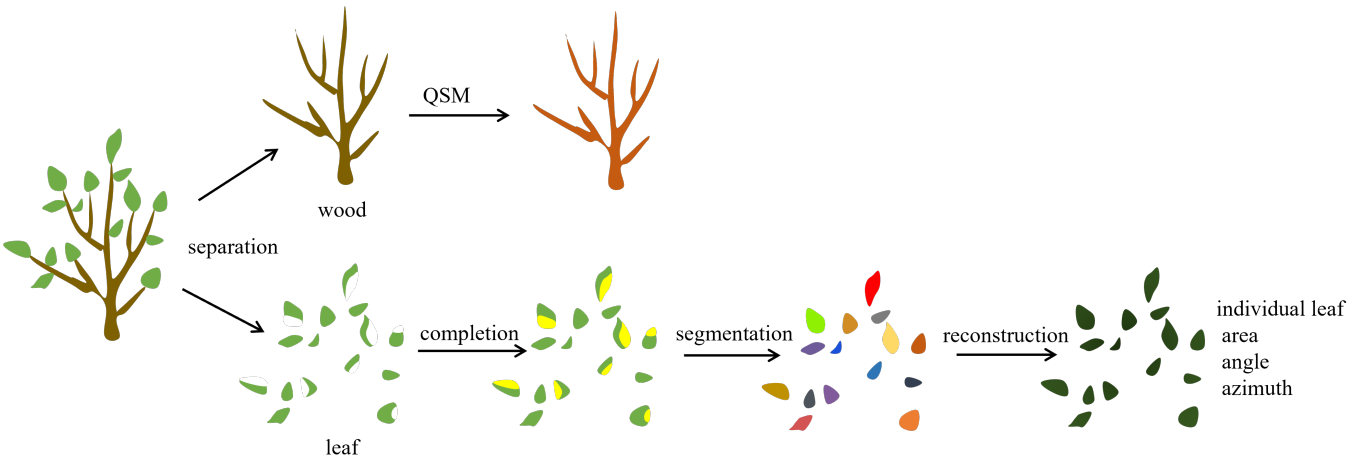

Fig. 1: Illustration of the proposed AdLeaf method.

A. TLS In-situ Tree Scanning

Our study site is a typical temperate deciduous broadleaf forest in northern China, located in Beijing. We scanned six trees of varying sizes using a Faro Focus^S 350 Plus (September and October 2022), as detailed in Table I. The scanning resolution was $10,240 \times 4,627$ (43.7 MPts) with a point spacing of 6.1 mm at a 10-meter distance. The scanning for each station was completed in 8 minutes. The registration and denoising of multi-station data for each tree were performed using FARO SCENE [61].

B. Leaf Data of Real Trees

Leaf samples. Following TLS scanning, 340 leaves (in total) were extracted from the point clouds of six trees (see Table I), with each leaf assigned a unique ID. To ensure distribution variability, each canopy was divided into upper, middle, and lower layers. Branches were randomly selected, and leaves were harvested in random order from bottom to top. To assess AdLeaf's performance in segmenting individual leaves, we manually isolated the point cloud data for each harvested leaf. Table I presents detailed statistical data on the manually collected leaves from the sampled trees.

Measurement of leaf areas. The leaf areas of the harvested leaves were measured using a handheld LI-3000C leaf area meter. This device employs an electronic rectangular approximation method with a resolution of 1 mm^2 and a scanning speed of 1 m/s. For leaf areas exceeding 10 cm^2, the error is less than 1%. This data was used to validate the leaf area measurements produced by AdLeaf.

TABLE I: Statistics on the 6 scanned trees and leaves.

Tree ID	Species	Height (m)	DBH (cm)	#Scans	#Total leaves	#Harvested leaves
1	Cherry	3.60	8.84	4	762	81
2	Cherry	2.50	5.96	4	343	27
3	Paper mulberry	7.80	12.01	3	1500	40
4	Poplar	15.50	22.99	3	4000	33
5	Poplar	3.70	2.51	2	201	50
6	Mulberry	2.70	2.10	2	1560	109

C. Leaf Data of Virtual Trees

We supplemented real data with synthetic point clouds generated through simulations, which allowed us to test configurations, identify biases, and mitigate human errors. To generate the synthetic leaf data, five 3D tree models were created in SpeedTree [62] with heights of 8 m, 13 m, 18 m, 23 m, and 28 m, respectively. Branches and leaves were customized by adjusting their number, size, position, and curvature to approximate natural conditions. The 3D tree models were then imported into HELIOS++ [63], where parameters were set to simulate the Riegl VZ-400 LiDAR platform, with a pulse frequency of 300 kHz, laser pulse length of 5 ns, laser emission frequency of 300,000 pts/s, scanning accuracy of 5 mm, and a maximum scanning angle of 120°. The simulated beams interact with the surfaces of the virtual trees, producing the point clouds.

TABLE II: Statistics on the synthetic trees and leaves.

Tree ID	Tree height (m)	#Leaves	Areas of simulated reference leaves (cm^2)
1	8	50	90, 50, 30, 40, 60
2	13	50	35, 85, 55, 50, 70
3	18	40	35, 70, 60, 45, 50
4	23	50	75, 30, 60, 70, 100
5	28	50	75, 55, 45, 50, 70

III. Methodology

As illustrated in Figure 1, the proposed AdLeaf method consists of four key steps: (1) wood-leaf separation (Section III-A), (2) leaf completion (Section III-C), (3) leaf instance segmentation (Section III-B), and (4) leaf reconstruction (Section III-D)

A. Wood-Leaf Separation

The core objective of AdLeaf is to achieve high-precision 3D reconstruction of individual leaves at the tree scale, which necessitates a sufficiently accurate classification of leaf-wood separated point clouds. Leaf-wood separation is a typical binary classification problem that requires labeling each point in the point cloud as either "wood" or "leaf". However, due to the frequent overlap and complex distribution of points belonging to leaves and woody components, traditional methods often fail to achieve fully automated and accurate separation, particularly at the boundaries between leaves and fine branches.

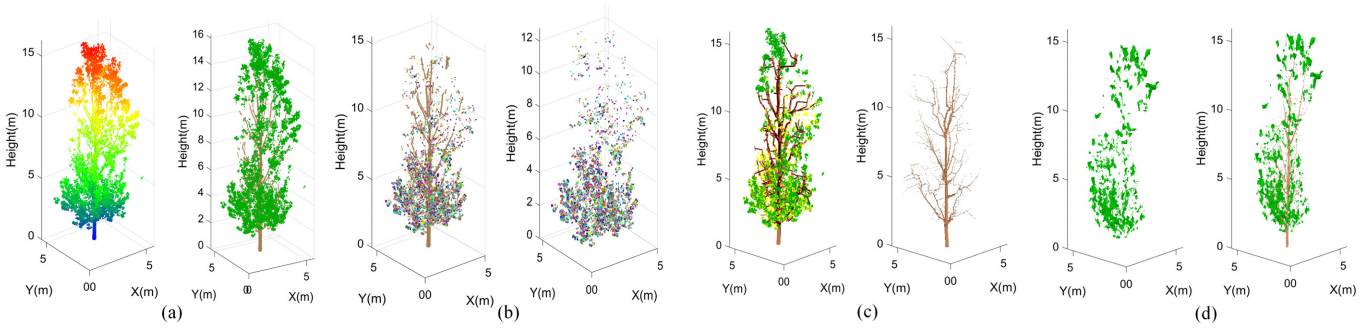

Fig. 2: AdLeaf is a key step in the quantitative reconstruction of individual leaves at the tree scale. (a) Wood-leaf separation; (b) Leaf instance segmentation; (c) Leaf completion; (d) Leaf reconstruction.

To address this challenge, we designed an efficient leaf-wood separation method for AdLeaf based on graph modeling and shortest-path optimization.

In the method design, we model the geometric relationships within the point cloud using a graph constructed with an adjacency list, where each point in the point cloud serves as a vertex of the graph, and the spatial distances between neighboring points are used as edge weights. This approach not only reduces memory consumption but also allows irrelevant vertex pairs to be skipped efficiently during graph traversal, thereby improving computational efficiency. The edge weights are defined as the squared Euclidean distance, which enhances the distinction for short distances while avoiding numerical precision issues. A KD-tree is employed for fast neighborhood searching, and edges are added between each point and its K nearest neighbors based on a distance threshold δ, ensuring a balance between computational efficiency and adaptability of the graph structure.

To achieve efficient separation, we focus on identifying the shortest path from each point to the tree trunk. Traditional shortest-path algorithms require calculating paths between all vertex pairs, with computational costs increasing dramatically as the point cloud size grows. To overcome this, we adopt the Shortest Path Faster Algorithm (SPFA) and incorporate optimization strategies, including Small Label First (SLF) and Large Label Last (LLL). Specifically, SLF prioritizes points with smaller distances, dynamically adjusting queue order to accelerate path relaxation, while LLL delays the processing of distant points to minimize redundant operations within the queue. These optimizations enable SPFA to achieve near-linear time complexity, significantly improving efficiency and scalability (see Algorithm 1 in the appendix).

To further enhance separation accuracy, we design a shortest-path backtracking strategy to correct misclassified leaf points connected to woody components. During the execution of SPFA, parent node information for each point is recorded to construct path arrays. Subsequently, leaf points identified as "end nodes", i.e., points with parent nodes but no further extensions, are traced back R steps along the path to remove potentially misclassified points. This strategy adjusts local connectivity, substantially improving the accuracy and robustness of the leaf-wood separation.

Additionally, to address misclassifications caused by the geometric similarity of secondary and fine branches to leaves, we incorporate point cloud normal vectors and curvature characteristics for further optimization. First, we calculate the covariance matrix using the 45 nearest neighboring points for each point and perform eigenvalue decomposition. The eigenvector corresponding to the smallest eigenvalue is extracted as the normal vector, while the curvature is defined based on the ratio of the eigenvalues to characterize the local geometric properties of the point. A curvature threshold (e.g., 0.03) is then applied to classify points with low curvature as woody points, effectively removing fine and secondary branch points and enhancing the accuracy of the leaf-wood separation.

We perform visual evaluations in 3D using CloudCompare. Points classified as wood, rather than leaves, are further separated. A manual inspection of branches and leaves is conducted to transfer any misclassified leaf points from branches to the correct leaf category (Fig. 3).

B. Leaf Instance Segmentation

AdLeaf segments individual leaves using a similarity graph where vertices represent points and edges reflect spatial relationships between the points. Based on this similarity graph structure, clusters corresponding to individual leaves are extracted by thresholding edge weights. Connected vertices form distinct clusters that are output as segmented leaves (see Fig. 4 and Algorithm 2 in the appendix).

Leaf segmentation is a critical step in quantitatively reconstructing individual leaves at the tree scale, aiming to independently isolate each leaf from the entire tree. During the segmentation process, the concept of connectivity-density hybrid segmentation is employed, where density clustering is first used for coarse segmentation, followed by graph-based optimization of connectivity to separate structures such as leaves, petioles, and twigs from the canopy point clouds. It involves two main stages: (1) initialization of segmentation instances and (2) instance segmentation based on similarity graphs. The AdLeaf algorithm ingeniously combines geometric modeling with graph-based methods, utilizing precise normal computation, 3D Delaunay triangulation, and similarity graph segmentation strategies. This approach effectively addresses the challenge of leaf segmentation in canopy point clouds, improving both segmentation accuracy and computational efficiency, particularly in complex canopy structures.

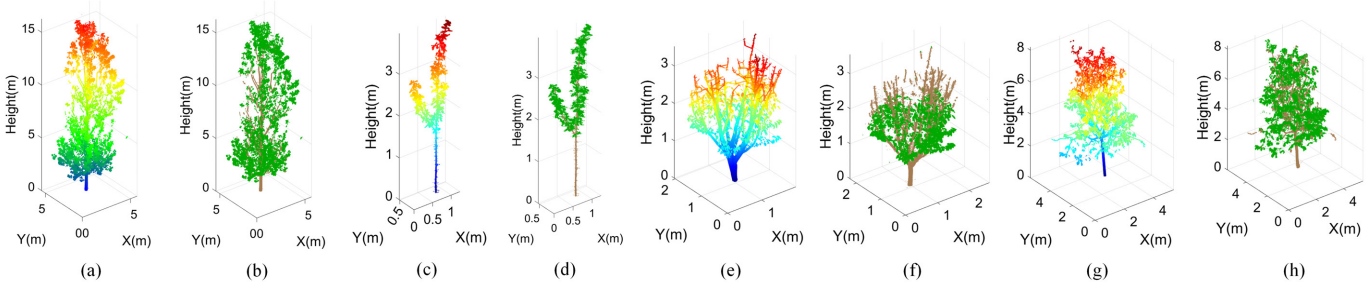

Fig. 3: Branch and leaf separation performed by both automatic and manual steps. (a), (c), (e), and (g) demonstrate tree point clouds (colored by height) before separation of branches and leaves; (b), (d), (f), and (h) show the corresponding point clouds with separated branches and leaves, which green color denotes non-woody structures and brown color woody structure.

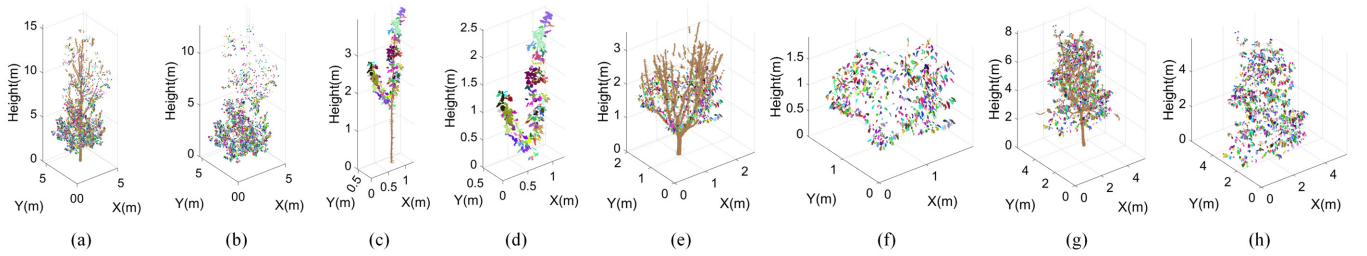

Fig. 4: Segmentation of all individual leaves at the tree level. (a), (c), (e), and (g) show individual leaves in different colors and wood structures in brown. (b), (d), (f), and (h) show the non-wooden structures in different colors after leaf separation.

1) Initialization of Segmentation Instances: This is the first step of AdLeaf's segmentation process, which primarily involves the computation of normals and poses. To accurately describe the geometric morphology and curvature of leaves, AdLeaf employs point cloud normal calculations. First, the algorithm traverses the entire canopy point cloud, selecting a reference point as the root node, and identifies its neighboring points using a KD-tree data structure. Within the local neighborhood, the algorithm computes the normal for each point by solving the covariance matrix to extract eigenvalues and eigenvectors, where the eigenvector corresponding to the smallest eigenvalue is taken as the normal vector. This process effectively captures the curvature information of the leaves, facilitating the subsequent identification of leaf shapes.

Next, AdLeaf performs 3D Delaunay triangulation on the canopy point cloud, converting the discrete points into a mesh. This step helps construct the canopy's topological structure, enabling more efficient processing of point cloud data. Each edge in the mesh is assigned a weight based on vertex attributes, with the weight calculation incorporating both the geometric distance between vertices and the angular difference between their normal vectors. Edges with lower weights indicate higher similarity between leaves, aiding in their identification. Delaunay triangulation ensures a more rational connection between points, thereby providing precise geometric data support for subsequent segmentation operations.

2) Leaf Segmentation Based on Similarity Graph: The similarity graph helps AdLeaf capture the geometric and normal vector similarities between leaves in the point cloud. After the initialization stage, AdLeaf constructs a similarity graph, where each point in the point cloud is treated as a vertex, and edges are constructed by calculating the similarity between points. The weight of each edge represents the geometric and normal vector similarity between points. Points with smaller normal vector angles and closer spatial distances are assigned lower weights, indicating a higher likelihood of belonging to the same leaf.

The similarity graph is constructed by connecting each point to both the source and sink nodes using t-links and connecting each point to its neighbors with n-links. This approach effectively captures similarity relationships within the point cloud, providing critical information for leaf segmentation. Once the similarity graph is built, AdLeaf assigns weights to each edge and uses a union-find algorithm to sort and merge edges in the graph. During this process, edges are traversed in ascending order of weight. If two vertices belong to different sets, their sets are merged; otherwise removed. This procedure effectively prevents misconnections between points from different leaves, ensuring segmentation accuracy. By applying a threshold, AdLeaf further reduces the number of edges, improving the connections between different leaves.

3) Leaf Clustering and Final Segmentation: Based on the similarity graph, AdLeaf performs final leaf segmentation through a clustering approach. The algorithm constructs a 3D similarity graph using edge weights and extracts individual leaf point clusters through thresholding operations on neighboring point weights. Specifically, AdLeaf searches each node's adjacency list in the similarity graph and assigns connected vertices to distinct leaf clusters according to a predefined threshold. By iterating through the leaf clusters in a double-loop manner, AdLeaf extracts the point set for

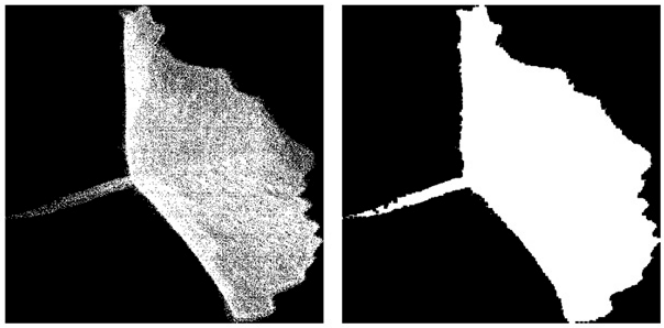

(a) Before closure (b) After closure

Fig. 5: Leaf point cloud closure and hole filling using the morphological operation.

each leaf. This process achieves accurate leaf segmentation, laying a solid foundation for subsequent leaf reconstruction and measurement.

C. Leaf Completion

At the tree scale, TLS scanning often results in incomplete leaf point clouds due to occlusions. To fully reconstruct a leaf and provide an accurate geometric shape, AdLeaf proposes a completion algorithm based on the principles of concavity, convexity, and symmetry. This algorithm consists of two main steps: (1) detection of incomplete leaves and (2) repair of incomplete leaves (see Algorithm 3 in the appendix).

1) Detection of Incomplete Tree Leaves: After leaf segmentation, we first identify incomplete leaf point clouds. To achieve this, AdLeaf leverages the concavity/convexity principle of a reference plane in conjunction with the spatial geometric information of the leaf point cloud to detect missing portions of the leaf. Initially, a statistical filter is applied to remove noise from the point cloud, ensuring detection accuracy. Then, the principal direction and centroid of the leaf point cloud are computed using the minimum bounding box principle (Eq. 1), which provides the global geometric information of the point cloud. Next, a reference plane is fitted, and the leaf point cloud is orthogonally projected onto a 2D plane (Eq. 2, Fig. 5), allowing the internal and external contours to be extracted. The centroid is computed as:

$$C = \frac{1}{n}\sum_{i=1}^{n} r_i \tag{1}$$

where C is the centroid vector, n is the number of points, and r_i is the position vector of each point. The orthogonal projection matrix P is calculated as:

$$P = I - \frac{\mathbf{n}\cdot\mathbf{n}^T}{\mathbf{n}^T\cdot\mathbf{n}} \tag{2}$$

where I is the identity matrix, and $\mathbf{n}$ is the plane's normal vector.

The grayscale values are normalized to the range 0 to 255, followed by a morphological closing operation to fill any holes in the image, ensuring a comprehensive reflection of the leaf's shape. On this basis, the convex hull algorithm is applied to calculate the maximum distance from the points to the convex hull, and the degree of damage is determined based on the percentage of the leaf area occupied by holes (Fig. 6). These methods, when combined, effectively identify incomplete leaves, especially in cases with large missing edges.

2) Repairing Incomplete Tree Leaves: Once incomplete leaves are identified, AdLeaf leverages the reflectional symmetry of leaves to infer the shape of the missing parts and perform geometric completion. First, the two most distant points on the leaf are selected, and the line connecting these points is used as the splitting line, dividing the leaf into two parts. Next, based on the concavity and convexity detection of each part, the algorithm determines which part is relatively complete. If both parts exhibit convex or concave shapes, the side with more points is selected as the source point cloud; if one side is convex and the other concave, the convex part is chosen as the source.

Then, Principal Component Analysis (PCA) is used to calculate the pose of the source point cloud, followed by an inverse matrix transformation to map the missing part of the point cloud. Through this approach, AdLeaf generates a symmetric point cloud for the missing part, and repairs the leaf's shape through relative position and structural matching (see Fig. 7).

3) Generation of Complete Leaves: To further refine the repair results, AdLeaf uses the minimum bounding rectangle to analyze the longest edges of the leaf and infer the axis of symmetry. The algorithm computes the vectors of the two longest edges and uses vector dot products to assess the distance of each non-zero point to the vector, thereby determining which points are closest to the axis of symmetry. AdLeaf generates the repaired point cloud by determining the most appropriate symmetry axis. Finally, the generated target point cloud is merged with the original point cloud to form a complete leaf. This entire repair process not only restores the missing portions of the leaf but also ensures the geometric consistency and natural shape of the leaf.

D. Leaf Reconstruction

The main goal of AdLeaf is to accurately construct the geometric model of the leaves from 3D point clouds. The process includes steps such as point cloud projection, geometric surface construction, mesh optimization, and smoothing. Through meticulous computation and precise geometric processing, AdLeaf reconstructs the true shapes of the leaves, providing a solid foundation for subsequent leaf parameter measurement (see Algorithm 4 in the appendix).

The reconstruction begins by projecting the leaf point cloud onto the best-fit plane. AdLeaf uses PCA to extract the principal directions of data distribution from the point cloud's covariance matrix, enabling dimensionality reduction. The algorithm first computes the geometric center of the point cloud and determines the principal axes of distribution. Then, it selects the eigenvector corresponding to the smallest eigenvalue as the normal vector of the fit plane. After this, the data center is aligned with the origin through translation, and the point cloud is projected onto the fitted plane to

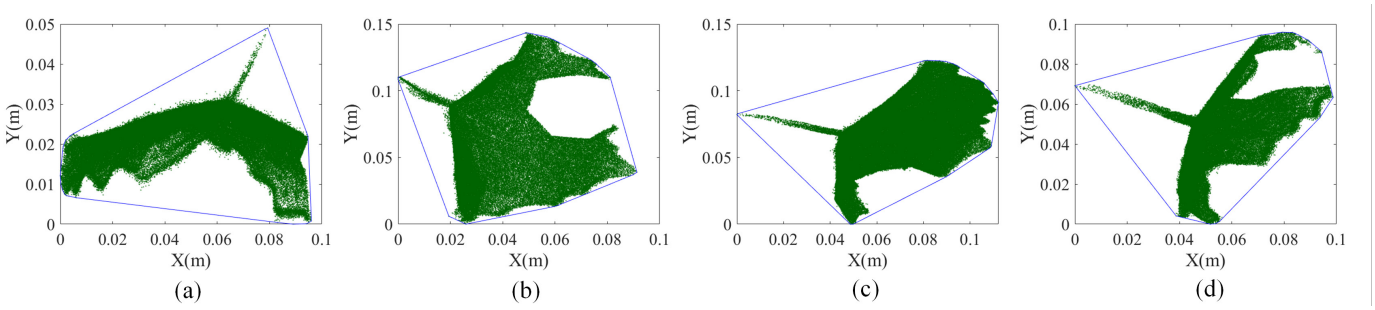

Fig. 6: Detection and identification of defective leaf point clouds. The blue outline in each subfigure indicates the convex hull of each leaf.

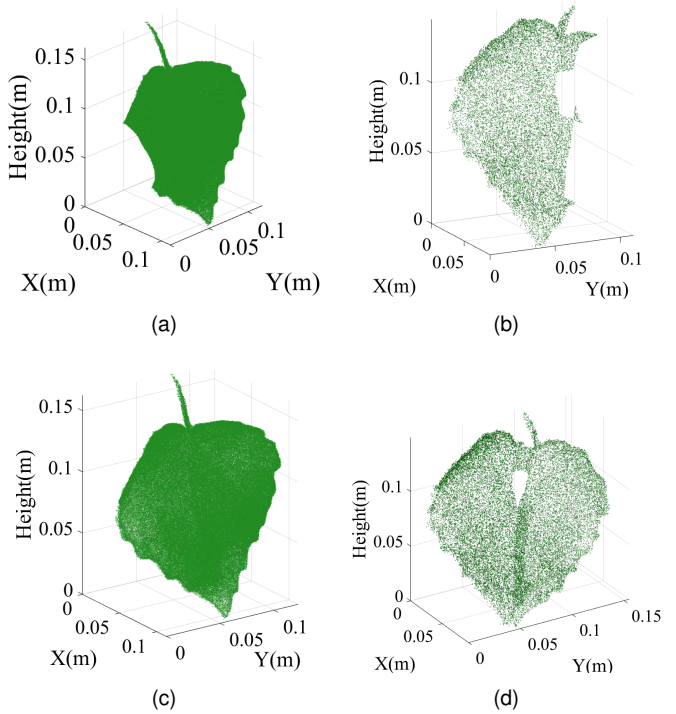

Fig. 7: Two leaf point clouds completed based on symmetry and concavity principles. Top row: Input incomplete leaf point clouds. Bottom row: Completion results.

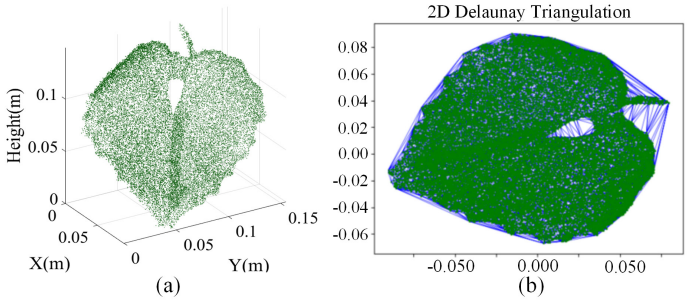

Fig. 8: A leaf point cloud (a) is projected onto a 2D plane (b).

generate a 2D geometric surface (as shown in Fig.8). With this, AdLeaf not only simplifies complex 3D data but also ensures that the fitted plane accurately reflects the main geometric features of the point cloud, simplifying the subsequent surface reconstruction.

Based on the 2D projection, AdLeaf uses Delaunay triangulation to mesh the projected points, which generates a basic surface mesh. This process optimizes the quality of the triangles, ensuring that each triangle meets the requirements for minimal angles and uniform edge lengths, thereby preventing large or irregular triangles from negatively affecting the reconstruction. For each triangle vertex, AdLeaf computes the vertex normal using a weighted average of the normals from neighboring triangles, ensuring the smoothness of the surface in the connecting regions. Then, through the fitting of geometric properties for each vertex and its normal, a continuous and smooth 3D surface mesh is generated. The surface mesh not only accurately reflects the geometric shape of the leaf but also undergoes spatial optimization during the fitting process, ensuring that each surface's position and orientation align with the actual leaf morphology, as shown in Fig. 9.

This process leverages the overall planarity of leaves to simplify reconstruction while ensuring the final 3D mesh retains the necessary geometric fidelity for downstream analyses. The methodology is efficient and robust, making it suitable for reconstructing the detailed structure of individual leaves from point clouds.

After generating the initial mesh, AdLeaf enhances the model quality by optimizing boundary surface elements. Specifically, the algorithm identifies and removes irregular large surface elements, especially abnormal triangles located at the boundary, by comparing the area of each triangle with the average area of its neighboring triangles. After that, the mesh is iteratively refined to ensure uniform distribution and continuity. Finally, to improve the smoothness of the leaf structure, AdLeaf applies the Laplacian smoothing algorithm to further adjust the mesh node positions. Through iterative adjustment, each node's position is optimized by combining a weighted average of neighboring nodes, improving the geometric structure and making the leaf surface smoother and more natural.

Once optimization is complete, AdLeaf maps the 2D surface mesh back to 3D space using affine transformations, restoring the original shape of the leaf. This process ensures the precise correspondence of geometric positions and orientations, while further optimizing the leaf surface curvature to ensure that the

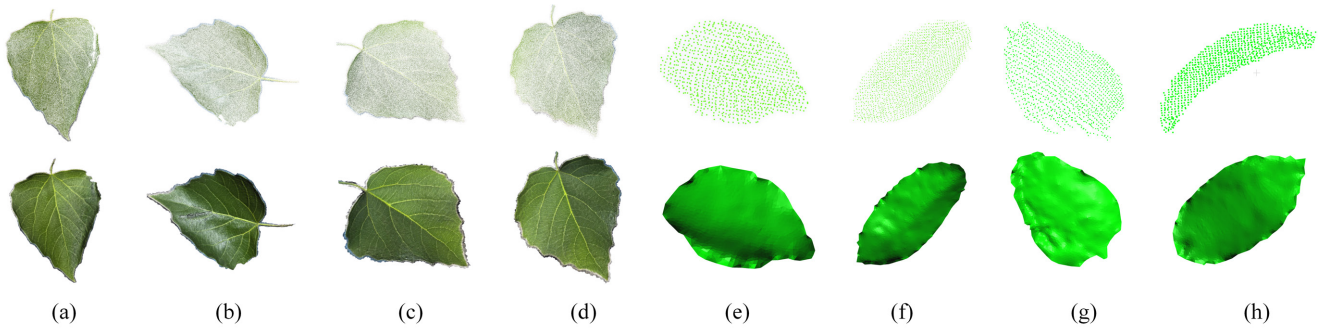

Fig. 9: Eight leaves reconstructed from point clouds. The first row shows the input leaf point clouds, and the second row shows the corresponding reconstructed mesh models. The points in (a) - (d) contain color information and are complete. In contrast, the points in (e) - (h) do not have color information and are incomplete, and thus leaf completion was performed before reconstruction.

reconstructed model better reflects the physical characteristics of the leaf. All steps adhere to the principles of geometric consistency and natural morphology, ultimately achieving the true restoration of the leaf's geometric structure and fine detail optimization.

E. Leaf Parameter Measurement

With the previously reconstructed leaf models, practical and application-relevant leaf measurements can be obtained, such as surface area, volume, leaf inclination angle, and azimuth angle. These measurements support plant morphology analysis, functional studies, and ecological modeling.

For the calculation of leaf inclination and azimuth angles, AdLeaf conducts geometric analysis based on point cloud normals. By computing the angle between the leaf point cloud's projection plane and the Z-axis, the leaf inclination angle is obtained, and the angle between the projection vector and the X-axis gives the azimuth angle. This method is straightforward and efficient, accurately describing the leaf's tilt direction and posture in 3D space, providing a reliable basis for analyzing its spatial distribution.

For surface area and volume calculation, AdLeaf employs a discrete algorithm based on the Gauss divergence theorem to process the leaf's 3D mesh model. To ensure accuracy, the algorithm divides the leaf surface into small, smooth regions, and the surface area is estimated by progressively calculating the change in the normal vectors between adjacent points. Additionally, the Maximum Unit Normal Component (MUNC) is introduced to optimize calculations, ensuring the consistency between local and total surface areas. For volume estimation, the algorithm processes the discrete point set using divergence theory, where the weighted sum of the normal vector gradients within each voxel is computed. This effectively reduces errors caused by small cross-sectional areas, thereby enabling high-precision volume estimation. This approach can handle irregular shapes of leaves while improving the reliability of the reconstructed models.

AdQSM is a method based on single-tree LiDAR point cloud data for constructing explicit wood structure models [64]. It accurately and comprehensively outputs structural models of wood components and a series of metrics [58]. When combined with AdLeaf (Fig. 10), AdQSM enhances the capability of TLS forest remote sensing in quantitatively reconstructing both woody and non-woody components of trees.

IV. Results

A. Effectiveness of AdLeaf in Measuring Leaf Count

AdLeaf utilizes instance segmentation of leaf point clouds within the canopy to count the leaves on an entire tree or branch. A field survey of leaf counts from seven samples (six trees and one branch) provided counts of 762, 343, 1500, 4000, 441, 201, and 1560, respectively. AdLeaf determined leaf counts of 771, 341, 1589, 4329, 415, 192, and 1484, with relative errors ranging from 0.58% to 8.23% (see Fig. 11). These results demonstrate AdLeaf's ability to accurately capture leaf numbers, with its performance showing no significant correlation with tree type, morphology, structure, or size.

B. Effectiveness of AdLeaf in Reconstructing Leaf Structure

We assess AdLeaf's accuracy in reconstructing leaf structures by calculating the average distance (AD) and standard deviation (SD) between the input point cloud and the generated leaf model. The results shown in Table III demonstrate that AdLeaf accurately reconstructs the non-woody structures of entire trees, closely matching natural trees. Generally, trees with high-density point clouds and broad leaves yield more accurate results. Figure 12 shows that, despite variations in shape, size, and structural complexity across trees, AdLeaf consistently delivers high reconstruction quality. Even with low sampling rates and relatively sparse point clouds, AdLeaf remains capable of generating visually reliable leaf models.

To further investigate sources of reconstruction error, we observed that discrepancies mainly originate from occlusion-induced incompleteness at leaf tips and petioles, scanner positioning errors, and under-segmentation in dense canopy regions. For Tree 2 and Tree 3, lower point density led to larger variation in fitted mesh surfaces, especially in overlapping leaf areas. This suggests that reconstruction accuracy is strongly affected by both the completeness and angular diversity of scans.

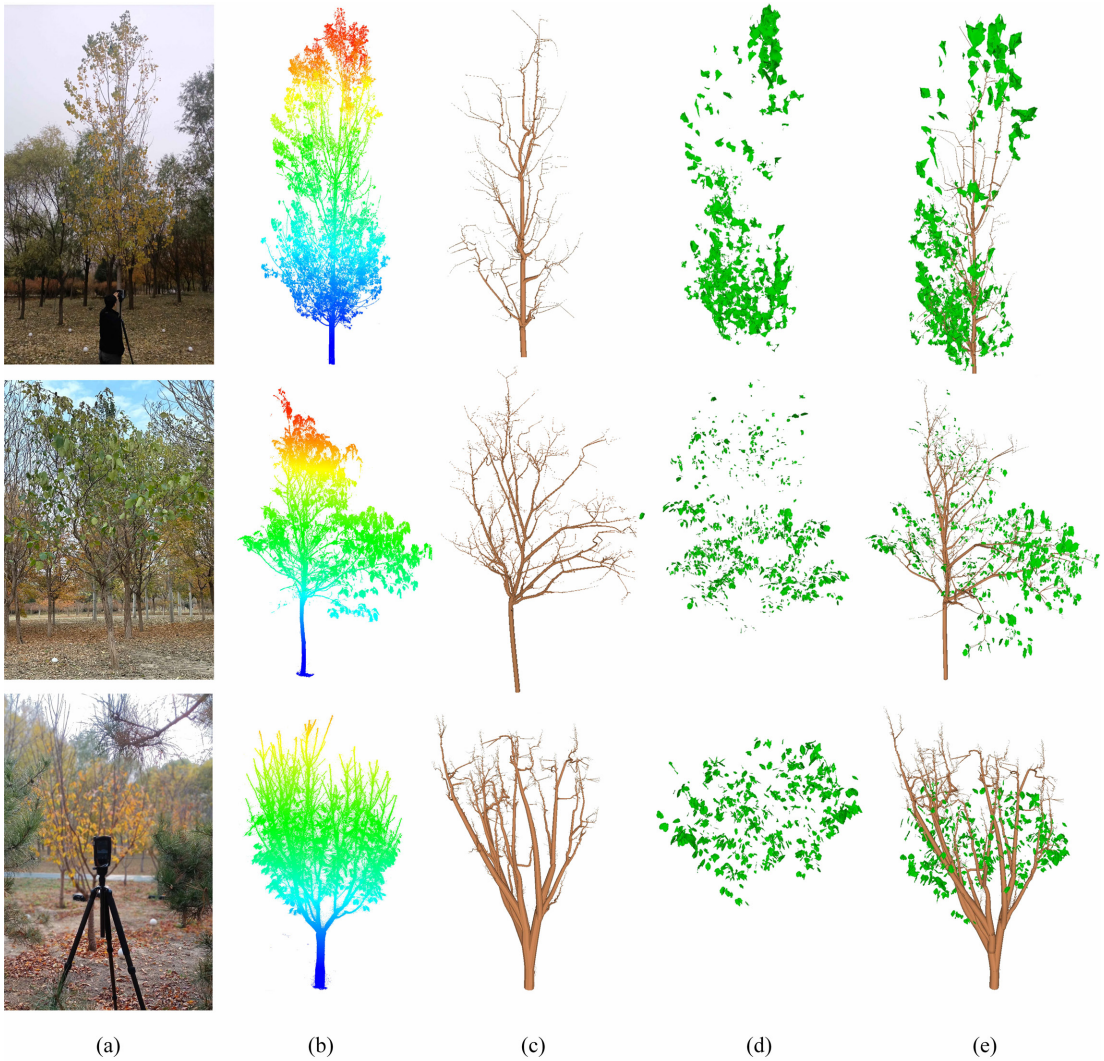

(a) (b) (c) (d) (e)

Fig. 10: Combining AdLeaf and QSM enables quantitative reconstruction of both woody and non-woody structures of trees. (a) Photos. (b) Trees point clouds. (c) Branches. (d) Reconstructed leaves. (e) Combining branches and leaves.

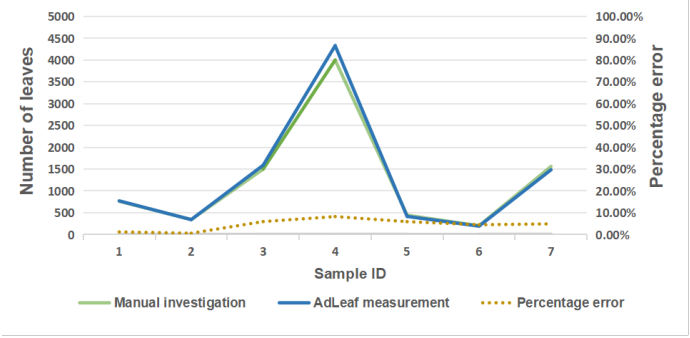

Fig. 11: Validity verification of leaf counting.

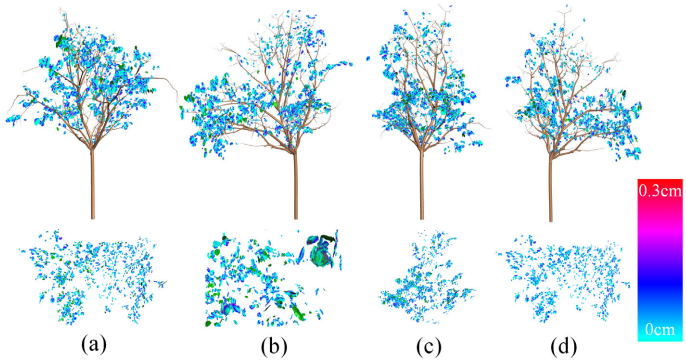

(a) (b) (c) (d)

Fig. 12: The distribution of reconstruction error (AD) measured on Tree 3. The subfigures demonstrate the complete tree model (top row) and the leaves only (bottom row) from different views.

Figure 13 visualizes the distributions of the errors of reconstructed leaves in terms of AD and SD, showing relatively stable AD and SD between 0.40 cm and 0.80 cm. High-quality reconstructions of non-woody structures by AdLeaf tend to perform better with trees that have higher-quality point clouds. As shown in Table III, the AD and SD between the point clouds and the reconstructed model surfaces are below 0.79 cm and 0.70 cm, respectively, demonstrating AdLeaf's ability to accurately reconstruct the non-woody structures of trees. The statistical results show that the AD values of all trees

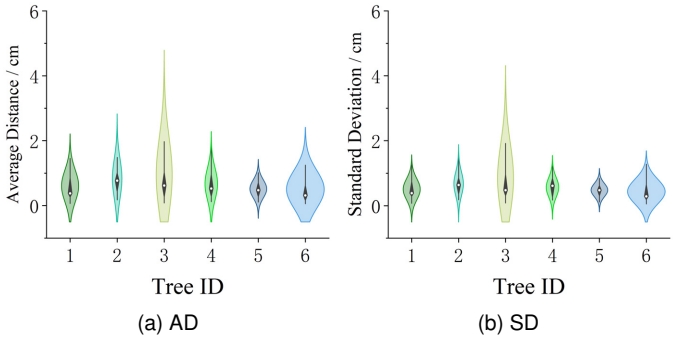

Fig. 13: Reconstruction accuracy (in terms of AD and SD) of the sampled trees. (a) AD. (b) SD.

TABLE III: Reconstruction accuracy (in terms of AD and SD) of sampled tree leaves.

Tree ID	Density (Pt/m^3)	#Point	AD (cm)	SD (cm)
1	117,189	816,255	0.61	0.51
2	66,871	753,364	0.83	0.68
3	29,193	577,431	0.79	0.70
4	308,876	857,157	0.67	0.57
5	70,879	7,517	0.52	0.48
6	122,939	89,494	0.50	0.44

TABLE IV: Accuracy of leaf areas of scanned trees of different species.

TreeID	Species	RMSE	rRMSE	Bias	rBias
1	Cherry tree a	4.90	15.60%	0.47	1.51%
2	Cherry tree b	3.88	13.07%	-1.21	-4.08%
3	Paper mulberry	8.04	11.77%	-2.21	-3.23%
4	Poplar tree	4.57	14.87%	2.01	6.54%
5	Poplar tree	5.26	15.71%	-0.11	-0.35%

remain below 0.83 cm. For trees with simpler structures, point errors tend to be smaller in the midsection or center of the leaf, while they are larger at the petiole or leaf tip. Overall, AdLeaf reliably reconstructs the non-woody structures of different trees, even when handling sparse point clouds.

C. Effectiveness of AdLeaf in Measuring Leaf Area

To verify the ability of AdLeaf in measuring leaf area, we investigate its accuracy using both real-scanned trees and simulated trees.

1) Measuring Leaf Areas of Scanned Trees: After scanning the trees, we measured the reference leaf area using a leaf area meter, with values ranging from 10 cm^2 to 180 cm^2, and compared them to the leaf areas reconstructed by AdLeaf, which ranged from 10 cm^2 to 170 cm^2. The reconstructed leaf areas closely match the reference values, achieving an R^2 of 0.95 and a slope of 0.93 (see Figure 14). The bias of the error is -0.20 cm^2, and the root mean square error (RMSE) is 5.63 cm^2. No significant change in error was observed as the reference values increased. Figure 15 shows the fitting results of AdLeaf's leaf area measurements against reference values for different trees, with accuracy details given in Table IV.

In addition to the evaluation on the tree level, this study also randomly sampled ten branches from five trees to evaluate the

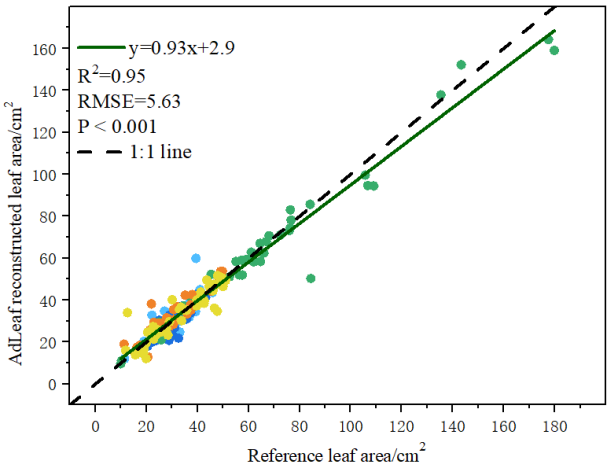

Fig. 14: Comparison of leaf areas between the values obtained by AdLeaf and ground truth, measured on different trees given in Table IV. The predictions are consistent across the range of leaf areas.

accuracy of the leaf area reconstruction by AdLeaf. Figure 16 presents the heat map of leaf area fitting coefficients for different branches of each tree, highlighting the high simulation accuracy, which aligns with the overall model performance. When reconstructing leaf areas from various parts of the trees, Broussonetia (Tree 3) exhibited the best simulation results, likely because of the superior quality of the point cloud obtained during the scanning process.

2) Measuring Leaf Areas of Simulated Trees: Besides the evaluation using real-scanned trees, we conducted tests on five trees with varying heights (simulated using HELIOS++), where the leaf areas were known. For instance, for an 8-meter-high tree, the leaf areas of branches A, B, C, D, and E were 90 cm^2, 50 cm^2, 30 cm^2, 60 cm^2, and 40 cm^2, respectively. The reconstructed leaf area by AdLeaf fell within 98% of the reference range (Fig. 17), demonstrating high accuracy, regardless of tree heights.

D. Effectiveness of AdLeaf in Repairing Incomplete Leaves

To assess AdLeaf's effectiveness in detecting and repairing incomplete leaves, we tested it on leaves from various trees. We compared the numbers of incomplete leaves detected by AdLeaf with the manually determined counts (Fig. 18). The results indicate that AdLeaf's detection error is under 28% across different tree samples, with smaller errors observed in trees with higher leaf counts. This suggests that AdLeaf performs more effectively as the number of leaves increases.

To evaluate AdLeaf's ability to repair incomplete leaves, we compared the leaf areas before and after repair with reference values. For the first five trees, the accuracy of the leaf area showed minimal change before and after completion. However, the accuracy for the sixth tree showed significant improvement (see Fig. 19). The relative root mean square error (rRMSE) of the leaf areas before and after completion was 79.7% and 70.3%, respectively, reflecting a 9.4% improvement in accuracy. AdLeaf's repair effect is particularly notable when

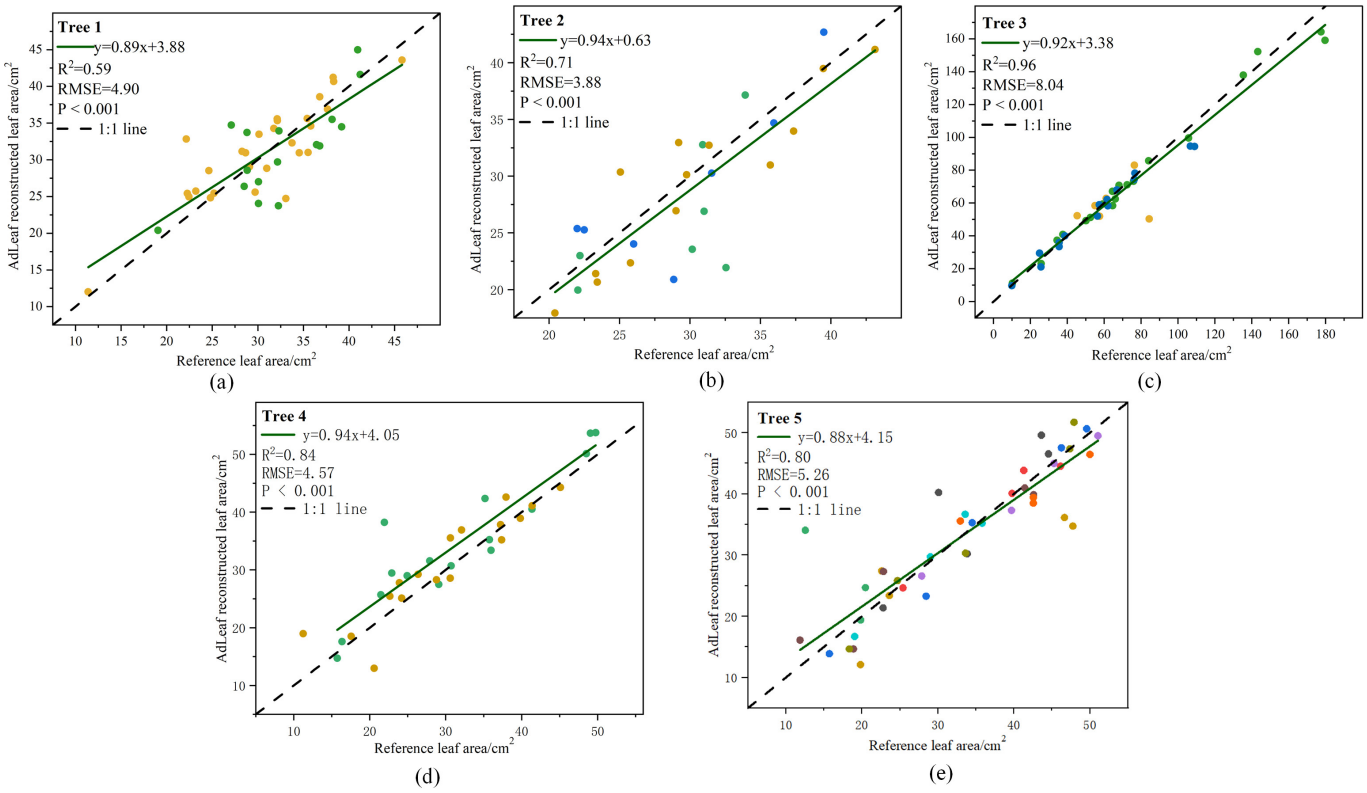

Fig. 15: Comparison of leaf areas between the values obtained by AdLeaf and ground truth. The subfigures correspond to the five trees in Table IV.

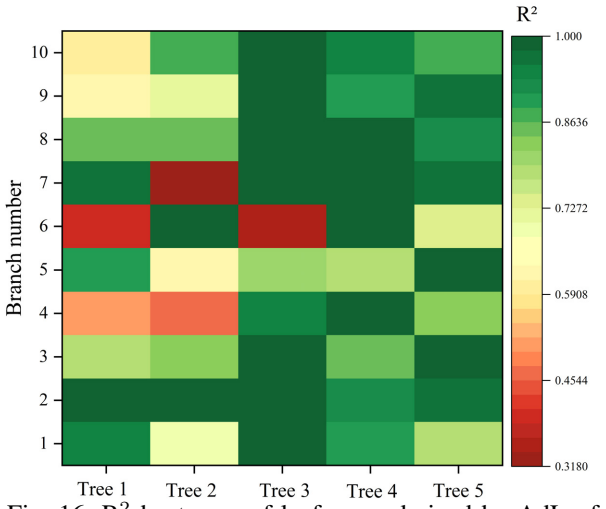

Fig. 16: R^2 heat map of leaf areas derived by AdLeaf.

the point cloud quality is low or the initial measurement accuracy is poor. The results further demonstrate that AdLeaf is especially effective in repairing large, severely damaged leaves, which is consistent with our visual interpretation that Tree 6 had notably more damaged leaves.

E. Quantitative 3D Visualization of Leaf Angle and Azimuth Distribution Reconstructed by AdLeaf

With AdLeaf, we also derived leaf angles and azimuths for the trees. Figures 20 and 21 demonstrate the distributions of the inclination and azimuth angles of the leaves, respectively. For these visualizations, we can observe that the leaves in the outer and lower parts of the canopy are nearly vertical, while those in the upper parts are more horizontal. The average azimuth angle tends to point toward the shortest path to the canopy's outer edge. Most leaf angles exceed 45°, and the azimuths are nearly parallel to the normal direction. In the upper canopy, leaves generally tilt southward at angles between 30° and 35°, optimizing solar interception (Bailey and Mahaffee, 2017). Meanwhile, leaves near the ground are almost vertical, oriented towards the canopy's outer edge, and absorb most of the sunlight.

AdLeaf reconstructs leaf angles to maximize sunlight interception. Leaves are oriented towards the normal direction and are more vertical, reflecting an optimal solar interception configuration. In the upper canopy, leaves tilt southward at angles between 30° and 35°, while those closer to the ground are more vertical, pointing towards the canopy's outer edge to capture more sunlight. The physical intuition and visualization in Fig. 21 support AdLeaf's measurement results. Overall, AdLeaf's leaf angle and azimuth measurements align with our observational findings.

V. Discussion

AdLeaf enables fine-scale reconstruction of non-woody tree structures, enhancing TLS capabilities beyond traditional QSM methods. AdLeaf's performance was assessed using scanned and simulated point clouds, in-situ measurements, and destructive sampling, focusing on: (a) leaf count accuracy; (b)

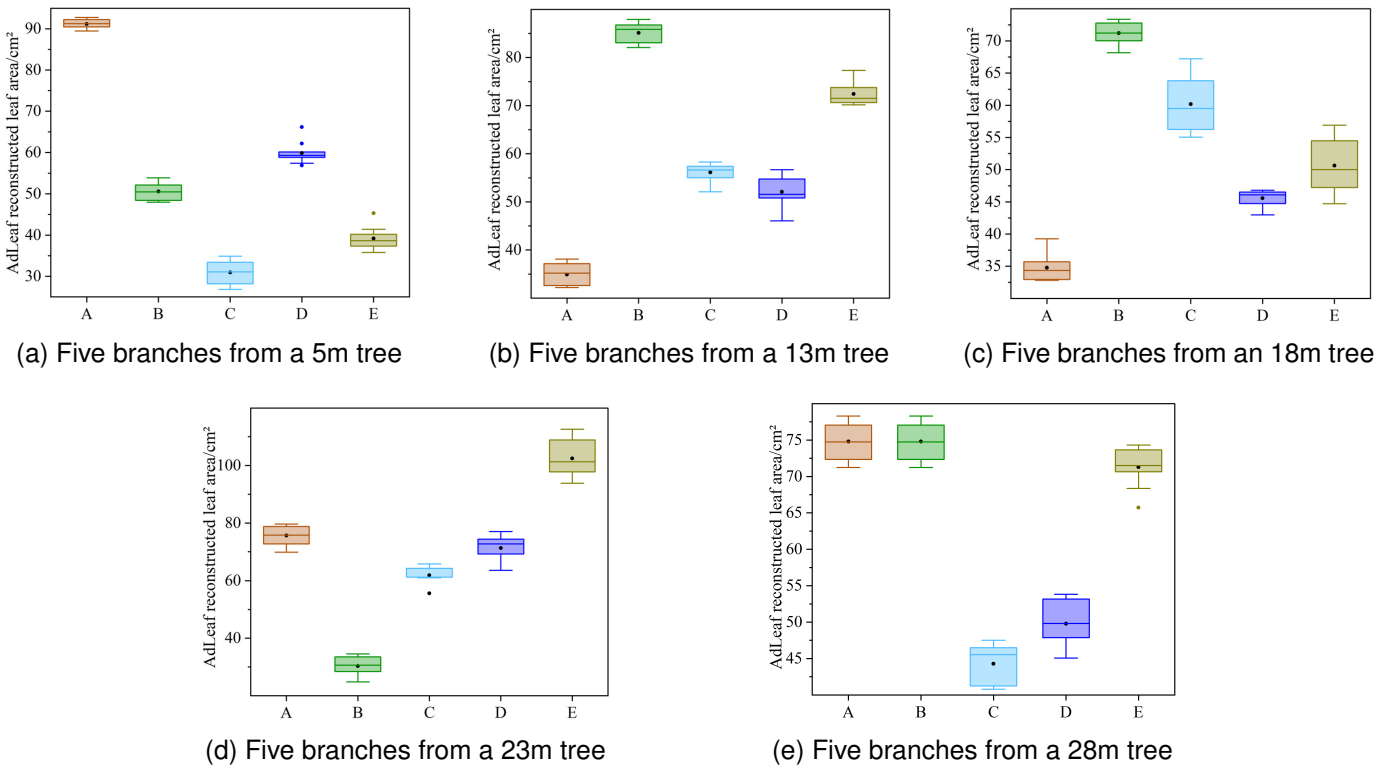

(a) Five branches from a 5m tree (b) Five branches from a 13m tree (c) Five branches from an 18m tree

(d) Five branches from a 23m tree (e) Five branches from a 28m tree

Fig. 17: The leaf area of synthetic trees of different heights. Each subfigure corresponds to the five branches of each tree given in Table II.

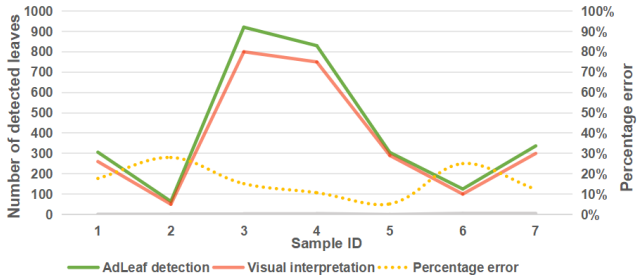

Fig. 18: Validity verification of defective leaf detection.

detection and repair of missing leaves; (c) geometric fidelity of non-woody structures and leaf area estimation; and (d) mapping of leaf inclination and azimuth distributions. The results highlight AdLeaf's ability to overcome limitations in existing QSM approaches.

A. Advantages in Quantitative Reconstruction of Tree Leaves

AdLeaf is a TLS-based quantitative reconstruction method that accurately models tree leaves, capturing attributes such as count, position, orientation, and area. It addresses spatial heterogeneity in canopy leaf distribution and supports species-independent leaf-level mapping and measurement. Field tests demonstrate a leaf count error of 0.58–8.23%, high geometric accuracy (with AD $<$ 0.83 cm and SD $<$ 0.70 cm), and robust leaf area estimation (R^2 = 0.95, Bias = -0.20 cm^2, RMSE = 5.63 cm^2). AdLeaf performs robustly even with lower-quality point clouds, though its geometric completion process may slightly reduce precision when data quality is high.

Unlike supervised deep learning approaches [20], [65], AdLeaf employs unsupervised instance segmentation, eliminating the need for labeled data while maintaining transparent, adjustable computations. It extracts multiple leaf attributes in a single pass. By advancing TLS capabilities to tree-level leaf measurement, AdLeaf introduces innovative reconstruction techniques, replacing simplified assumptions in forest remote sensing and contributing significantly to TLS-based forest ecology research.

B. Runtime Efficiency of AdLeaf

All experiments were conducted on a computer equipped with a 12th Gen Intel (R) Core (TM) i5-12500H processor and 16 GB RAM. On average, AdLeaf processed each of six scanned trees in about 70 seconds. While suitable for single-tree analysis, scaling to plot-level reconstructions introduces computational challenges. Future improvements will include downsampling, prioritized clustering, and parallel batch processing to enhance scalability.

C. Challenges and Influencing Factors in Leaf Reconstruction

AdLeaf mitigates reconstruction errors caused by poor segmentation or improper leaf fitting. Assuming effective separation of leaves from branches, AdLeaf employs graph combination and shortest path backtracking for automatic segmentation and quality control. Using a graph-cut framework, the

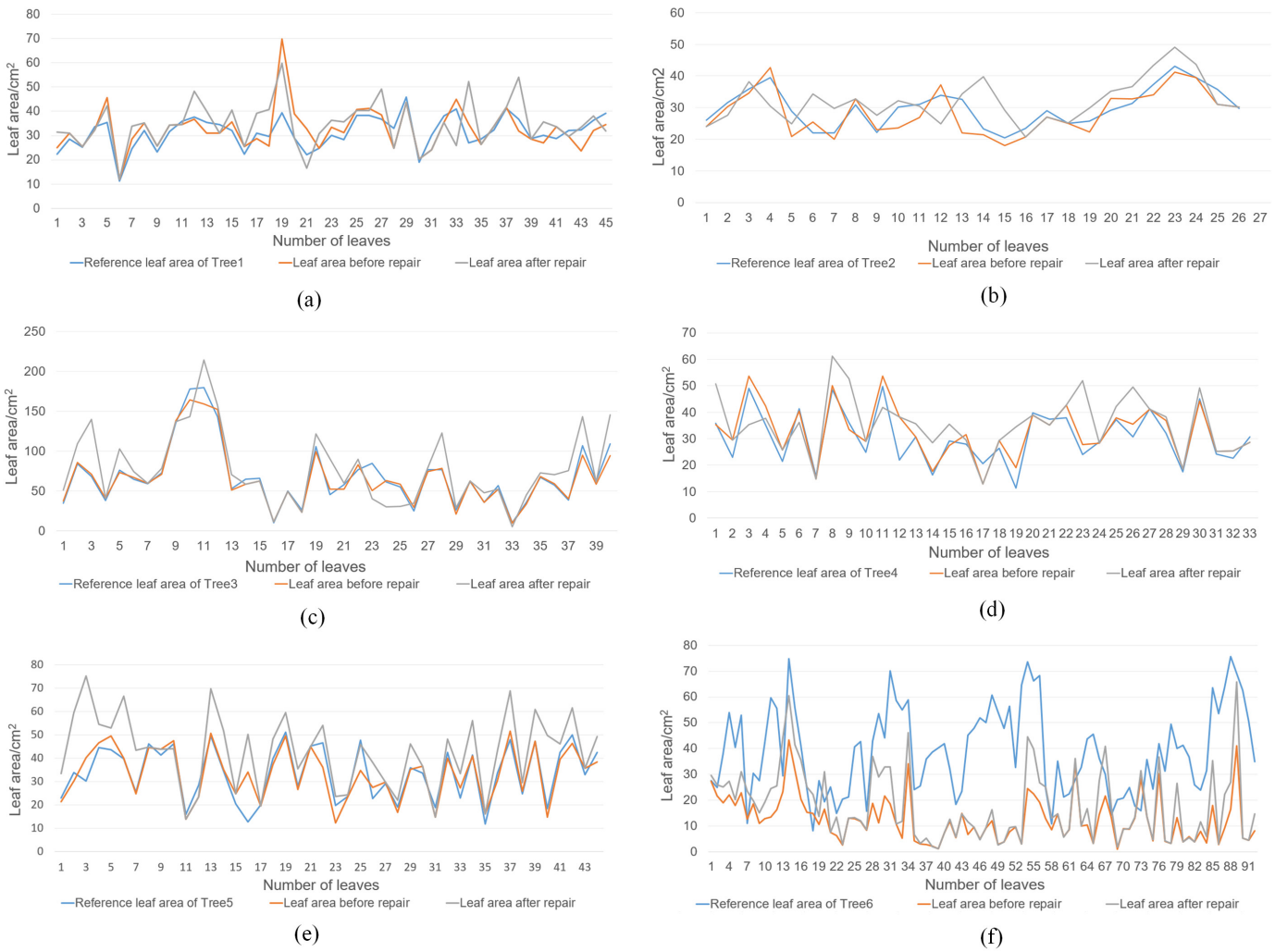

Fig. 19: Effect of leaf completion on leaf area estimation.

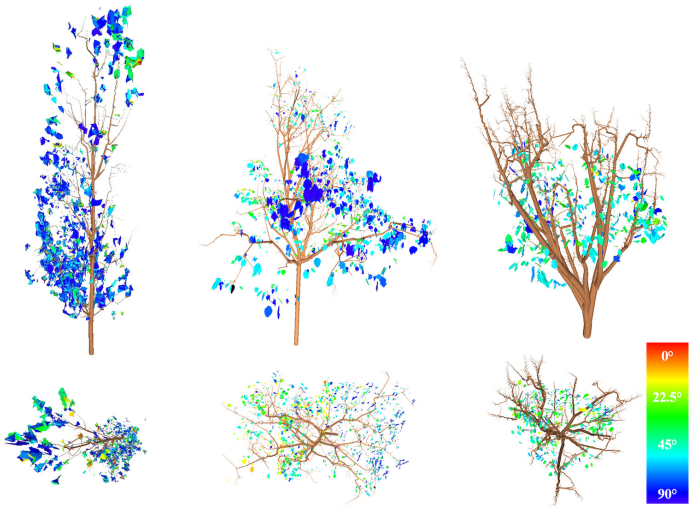

Fig. 20: Visualization of the distribution of leaf angles of three randomly selected trees. Top: side view. Bottom: the corresponding top view of the canopy.

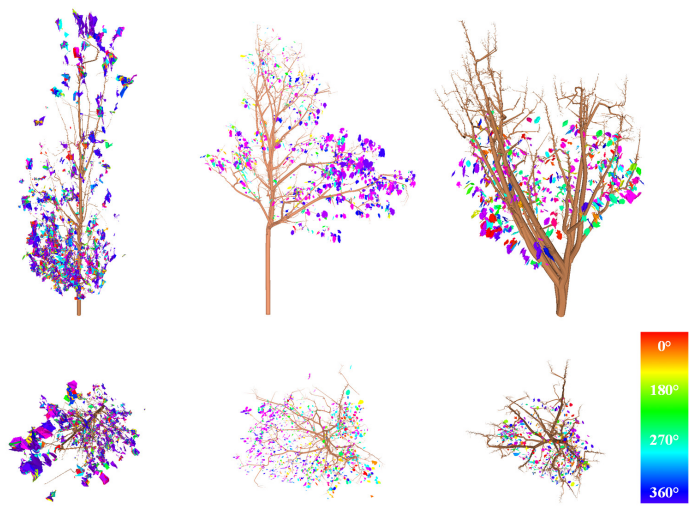

Fig. 21: Visualization of the distribution of azimuth corners of the same trees in Figure 20. Top: side view. Bottom: the corresponding top view of the canopy.

method leverages topological relationships and edge weights to segment leaves, while its core surface reconstruction relies on additional assumptions and constraints for accurate processing.

To resolve reconstruction issues, AdLeaf incorporates a 3D geometric completion algorithm and a leaf parameter estimation framework. This framework repairs incomplete or missegmented leaves based on symmetry and concavity principles. The axis connecting the two furthest points may not represent true biological symmetry, especially in broad or irregular leaves. AdLeaf treats this as a geometric approximation to support robust bilateral segmentation. Reconstruction quality is highly dependent on input point cloud resolution and completeness, which are influenced by scanner specifications and canopy structure [66], [67].

For leaf area estimation, lower-quality point clouds (often affected by occlusion) reduce sensitivity, particularly under high leaf density or ambiguous positions [68], [69]. Absolute errors are greatest with poor-quality data, but overall area size is less impacted. Despite variations across tree species, AdLeaf achieves robust quantitative reconstruction of non-woody structures, with measurement precision influenced by scanner accuracy, tree height, and canopy occlusion.

The AdLeaf pipeline includes branch-leaf separation, leaf segmentation, damaged leaf completion, structural reconstruction, and parameter estimation, each sensitive to point cloud quality but tunable for performance gains. Enhanced branch-leaf separation, for instance, ensures smoother leaf area distribution and consistent canopy measurements.

Leveraging TLS technology, AdLeaf effectively processes high-resolution point clouds and holds potential for integration with multi-sensor or multi-source point cloud fusion technologies. Future advancements in these areas will further enhance its capabilities, making it a powerful tool for forest remote sensing.

D. Limitations and Potential of AdLeaf

AdLeaf offers a practical solution for close-range forest remote sensing, enabling detailed reconstruction of non-woody tree structures. Its performance depends on the quality of point clouds, influenced by TLS instrument capability, scan resolution, number of stations, duration, and canopy accessibility. A typical scan takes around 10 minutes, with longer times required for large or dense trees.

AdLeaf can reconstruct partially scanned leaves but shows reduced accuracy as data gaps widen. Reliable reconstruction generally requires at least 50% leaf surface coverage. Below one-third, convex hull-based defect detection becomes unreliable. Enhancing robustness under extreme occlusion is a key direction for future work. Challenges include filtering, noise suppression, wood–leaf separation, segmentation, and repair accuracy. Though not yet applicable to conifers, AdLeaf advances TLS-based tree measurements to the leaf scale, supporting new opportunities in vegetation modeling and ecological analysis.

AdLeaf requires few input parameters, and its branch pretraining supports intuitive parameter tuning for leaf segmentation. The estimated leaf areas and orientations closely align with actual measurements. By integrating wood structure models from QSM [64], AdLeaf enables seamless scaling from leaf to canopy without assuming homogeneity, enhancing insights into structure-function relationships [1].

Although validated in temperate broadleaf environments, AdLeaf's geometric modeling and unsupervised segmentation are theoretically extendable to other broadleaf forest types. For tropical or coniferous forests, adaptations such as denser scanning and tailored segmentation thresholds may be necessary. Future work will extend validation to evergreen and needleleaf environments to enhance generalizability. Ongoing improvements include higher-resolution scanning, integration with ULS data, and broader applications such as radiative transfer modeling and physiological studies [53]. In summary, AdLeaf represents a promising step toward fine-scale ecological analysis and forest remote sensing.

VI. Conclusion

This study presents a theoretical and practical framework for quantitatively reconstructing tree photosynthetic components using TLS point clouds. The proposed AdLeaf method enables explicit modeling of individual leaves at the tree level. By overcoming QSM limitations, AdLeaf transitions from traditional virtual canopy representations to explicit, quantitative modeling of individual leaves. This approach provides critical leaf structural parameters essential for understanding forest functions and environmental processes under climate change.

AdLeaf captures heterogeneous leaf geometry, including 3D inclination and azimuth, supporting analysis of light interception and resource allocation. Combined with QSM, it enables comprehensive TLS-based measurement of both woody and leafy structures, improving plant functional models and reducing uncertainty in close-range sensing. The explicit 3D outputs of AdLeaf are compatible with other remote sensing modalities (e.g., imagery). Future directions include fusing AdLeaf outputs with UAV LiDAR for multiscale canopy monitoring and integrating with hyperspectral imagery to assess leaf-level photosynthetic activity and forest health.

Acknowledgments

We would like to thank all related personnel for their support and help in this study, and the reviewers for their constructive feedback. This work was supported by Investigating the Spatiotemporal Variations and Influencing Factors of Vegetation Carbon Sequestration Capacity in the Three-North Shelterbelt of Kubuqi Desert (KF2024MS03), Study on the Spatiotemporal Evolution Characteristics and Driving Mechanisms of Forest Carbon Storage in Southwest China (TDSYS202403), Mangrove species identification and growth monitoring and early warning based on the combination of UAV hyperspectral image and LiDAR point clouds (2024GXLK08), and The National Postdoctoral Innovative Talents Support Plan China Postdoctoral Science Foundation (BX20220038).

Appendix

Algorithm 1 SLF+LLL optimized SPFA algorithm

Input: point clouds of a single tree
Output: wood and leaf points

// Constructing Distance-Based Graphs for Point Clouds
function ConstructGraph(treeCloud, delta, k)
$graph \leftarrow$ initialize with size $|treeCloud|$
for $i \leftarrow 1$ to $|treeCloud.points|$ **do**
  $(indices, dists) \leftarrow kdtree.knnSearch(treeCloud.points[i], k)$
  for $j \leftarrow 1$ to k **do**
    if $dists[j] \leq delta^2$ **then**
      $graph[i].addEdge(indices[j])$
    end if
  end for
end for
return $graph$
end function

//Extracting the shortest path using the SPFA optimized with SLF and LLL
function SPFA(graph)
$distance \leftarrow$ array initialized to ∞
$queue, inQueue, countInQueue \leftarrow$ empty structures
$weightSum \leftarrow 0$
while queue not empty **do**
  $u \leftarrow queue.front()$
  $queue.pop()$
  for each neighbor v of u **do**
    if $distance[v] > distance[u] + weight(u, v)$ **then**
      $distance[v] \leftarrow distance[u] + weight(u, v)$
      if $v \notin queue$ **then**
        if $countInQueue[v] == 0$ **or** LLL_condition **then**
          $queue.push\_front(v)$ {LLL operation}
        else
          $queue.push\_back(v)$ {SLF operation}
        end if
      end if
      $inQueue[v] \leftarrow$ true
      $countInQueue[v] \leftarrow countInQueue[v] + 1$
    end if
  end for
end while
end function

Algorithm 2 Individual leaf segmentation

Input: Point clouds of all leaves from a single tree
Output: Individual leaf point clouds
function IndividualLeafSegmentation(points, radius, threshold)
// Initialize and compute normals
$normals \leftarrow computeNormals(points, radius)$
// Build similarity graph
$triMesh \leftarrow perform3DTriangulation(points)$
$edgeList \leftarrow buildSimGraph(triMesh)$
// Calculate edge weight threshold
$eTs \leftarrow calcMean(edgeList.weights)$ + $threshold \times calcStdDev(edgeList.weights)$

// Segment leaves
$leafClusters \leftarrow individualLeaves(points, edgeList, eTs)$
return $leafClusters$
end function
function computeNormals(points, radius)
for each $p \in points$ **do**
$neighbors \leftarrow findNeighbors(p, points, radius)$
$normal[p] \leftarrow pcaNormalEstimation(neighbors)$
end for
return $normals$
end function

function individualizeLeaves(points, edgeList, threshold)
$adjList \leftarrow obtainAdjSimGraph(edgeList, threshold)$
$clusters \leftarrow connectedComponents(adjList)$
return $clusters$
end function

REFERENCES

[1] M. Abegg, R. Bösch, D. Kükenbrink, and F. Morsdorf, "Tree volume estimation with terrestrial laser scanning—testing for bias in a 3d virtual environment," *Agricultural and Forest Meteorology*, vol. 331, p. 109348, 2023.

[2] G. Arseniou, D. W. MacFarlane, K. Calders, and M. Baker, "Accuracy differences in aboveground woody biomass estimation with terrestrial laser scanning for trees in urban and rural forests and different leaf conditions," *Trees*, vol. 37, no. 3, pp. 761–779, 2023.

[3] R. Darvishzadeh, C. Atzberger, A. Skidmore, and M. Schlerf, "Mapping grassland leaf area index with airborne hyperspectral imagery: A comparison study of statistical approaches and inversion of radiative transfer models," *ISPRS Journal of Photogrammetry and Remote Sensing*, vol. 66, no. 6, pp. 894–906, 2011.

[4] G. B. West, J. H. Brown, and B. J. Enquist, "A general model for the origin of allometric scaling laws in biology," *Science*, vol. 276, no. 5309, pp. 122–126, 1997.

[5] C. A. Price, B. J. Enquist, and V. M. Savage, "A general model for allometric covariation in botanical form and function," *Proceedings of the National Academy of Sciences*, vol. 104, no. 32, pp. 13 204–13 209, 2007.

[6] C. A. Price, K. Ogle, E. P. White, and J. S. Weitz, "Evaluating scaling models in biology using hierarchical bayesian approaches," *Ecology letters*, vol. 12, no. 7, pp. 641–651, 2009.

[7] Q. Guo, Y. Su, and T. Hu, *LiDAR principles, processing and applications in forest ecology*. Academic Press, 2023.

[8] A. Chlus, E. L. Kruger, and P. A. Townsend, "Mapping three-dimensional variation in leaf mass per area with imaging spectroscopy and lidar in a temperate broadleaf forest," *Remote Sensing of Environment*, vol. 250, p. 112043, 2020.

[9] M. B. Vicari, M. Disney, P. Wilkes, A. Burt, K. Calders, and W. Woodgate, "Leaf and wood classification framework for terrestrial lidar point clouds," *Methods in Ecology and Evolution*, vol. 10, no. 5, pp. 680–694, 2019.

[10] S. E. Reutebuch, H.-E. Andersen, and R. J. McGaughey, "Light detection and ranging (lidar): an emerging tool for multiple resource inventory," *Journal of forestry*, vol. 103, no. 6, pp. 286–292, 2005.

[11] Q. Guo, Y. Su, T. Hu, H. Guan, S. Jin, J. Zhang, X. Zhao, K. Xu, D. Wei, M. Kelly *et al.*, "Lidar boosts 3d ecological observations and modelings: A review and perspective," *IEEE Geoscience and Remote Sensing Magazine*, vol. 9, no. 1, pp. 232–257, 2020.

[12] H. Chen, F. Gao, Q. Zhu, Q. Yan, D. Hua, and S. Stanič, "Storage method of multi-channel lidar data based on tree structure," *Scientific Reports*, vol. 12, no. 1, p. 9075, 2022.

Algorithm 3 Detecting and repairing incomplete leaves

Input: Leaf point clouds
Output: Complete and completed leaves

$IncompletLeaves \leftarrow$ input leaf clouds
//Calculate the orientation and centroid of the leaves
$(centroid, vector) \leftarrow vectorAndCentroid(Cloud)$
$transform \leftarrow toAffine3f(vector, centroid)$
//Calculate the projection plane
$(mask, depthImg) \leftarrow pointCloudToImg(inputCloud, scale)$
$cleaned \leftarrow statisticalOutlier(inputCloud, 50, 1.0)$
//Detect incomplete leaves
$defects \leftarrow convexityDefects(mask, ratio, min, max)$

//Repair incomplete leaves
function fix_defect(id, cloud, config)
$(left, right) \leftarrow splitLeftRight(cloud)$
$L \leftarrow checkDefect(id, left, config)$
$R \leftarrow checkDefect(id, right, config)$
if L **or** R **then**
  $side \leftarrow$ larger of $(left, right)$
end if
$result \leftarrow$ new PointCloud()
for $point \in side$ **do**
  $result.push\_back(point)$
end for
return $result$
end function

Algorithm 4 Explicit reconstruction of leaf model

Input: leaf_cloud - individual leaf point clouds
Output: mesh - 3D explicit model of the leaf

function reconstruct(leaf_cloud):
// Compute best projection plane via PCA
pca.fit($points$)
plane $\leftarrow$ (pca.center, pca.normal)
// Project points to 2D
for $i \leftarrow 1$ to $|points|$ **do**
  $projections[i] \leftarrow$ plane.to2d($points[i]$)
end for
// Triangulate projections
$delaunay$.set_vertices($projections$)
// Build mesh from triangulation
for $i \leftarrow 1$ to $|points|$ **do**
  $mesh$.add_vertex($points[i]$)
end for
// Transfer vertex colors
$cloud\_colors \leftarrow leaf\_cloud$.get_colors()
$mesh\_colors \leftarrow mesh$.add_color_property()
for $t \leftarrow 1$ to $delaunay$.nb_triangles() **do**
  $vts \leftarrow$ empty list
  for $j \leftarrow 1$ to 3 **do**
    $v \leftarrow delaunay$.tri_vertex(t, j)
    if $v \geq 0$ **then**
      vts.push_back(v)
      $mesh\_colors[v] \leftarrow cloud\_colors[v]$
    end if
  end for
  $mesh$.add_face(vts)
end for
return $mesh$
end function

[13] J. Liu, A. K. Skidmore, T. Wang, X. Zhu, J. Premier, M. Heurich, B. Beudert, and S. Jones, "Variation of leaf angle distribution quantified by terrestrial lidar in natural european beech forest," *ISPRS journal of photogrammetry and remote sensing*, vol. 148, pp. 208–220, 2019.

[14] J. Guillemot, M. Kunz, F. Schnabel, A. Fichtner, C. P. Madsen, T. Gebauer, W. Härdtle, G. von Oheimb, and C. Potvin, "Neighbourhood-mediated shifts in tree biomass allocation drive overyielding in tropical species mixtures," *New Phytologist*, vol. 228, no. 4, pp. 1256–1268, 2020.

[15] S. Jay, F. Baret, D. Dutartre, G. Malatesta, S. Héno, A. Comar, M. Weiss, and F. Maupas, "Exploiting the centimeter resolution of uav multispectral imagery to improve remote-sensing estimates of canopy structure and biochemistry in sugar beet crops," *Remote Sensing of Environment*, vol. 231, p. 110898, 2019.

[16] J. Pisek, O. Borysenko, R. Janoutová, and L. Homolová, "Estimation of coniferous shoot structure by high precision blue light 3d photogrammetry scanning," *Remote Sensing of Environment*, vol. 291, p. 113568, 2023.

[17] B. Brede, L. Terryn, N. Barbier, H. M. Bartholomeus, R. Bartolo, K. Calders, G. Derroire, S. M. K. Moorthy, A. Lau, S. R. Levick *et al.*, "Non-destructive estimation of individual tree biomass: Allometric models, terrestrial and uav laser scanning," *Remote Sensing of Environment*, vol. 280, p. 113180, 2022.

[18] X. Liu, Y. Su, T. Hu, Q. Yang, B. Liu, Y. Deng, H. Tang, Z. Tang, J. Fang, and Q. Guo, "Neural network guided interpolation for mapping canopy height of china's forests by integrating gedi and icesat-2 data," *Remote Sensing of Environment*, vol. 269, p. 112844, 2022.

[19] M. Disney, "Terrestrial li dar: a three-dimensional revolution in how we look at trees," *New Phytologist*, vol. 222, no. 4, pp. 1736–1741, 2019.

[20] S. Wei, T. Yin, M. A. Dissegna, A. J. Whittle, G. L. F. Ow, M. L. M. Yusof, N. Lauret, and J.-P. Gastellu-Etchegorry, "An assessment study of three indirect methods for estimating leaf area density and leaf area index of individual trees," *Agricultural and Forest Meteorology*, vol. 292, p. 108101, 2020.

[21] Y. Li, Q. Guo, Y. Su, S. Tao, K. Zhao, and G. Xu, "Retrieving the gap fraction, element clumping index, and leaf area index of individual trees using single-scan data from a terrestrial laser scanner," *ISPRS Journal of Photogrammetry and Remote Sensing*, vol. 130, pp. 308–316, 2017.

[22] X. Wang, H. Xiang, W. Niu, Z. Mao, X. Huang, and F. Zhang, "Oblique photogrammetry supporting procedural tree modeling in urban areas," *ISPRS Journal of Photogrammetry and Remote Sensing*, vol. 200, pp. 120–137, 2023.

[23] I. Shlyakhter, M. Rozenoer, J. Dorsey, and S. Teller, "Reconstructing 3d tree models from instrumented photographs," *IEEE Computer Graphics and Applications*, vol. 21, no. 3, pp. 53–61, 2001.

[24] J.-F. Côté, J.-L. Widlowski, R. A. Fournier, and M. M. Verstraete, "The structural and radiative consistency of three-dimensional tree reconstructions from terrestrial lidar," *Remote Sensing of Environment*, vol. 113, no. 5, pp. 1067–1081, 2009.

[25] J.-F. Côté, R. A. Fournier, and R. Egli, "An architectural model of trees to estimate forest structural attributes using terrestrial lidar," *Environmental Modelling & Software*, vol. 26, no. 6, pp. 761–777, 2011.

[26] S. Delagrange and P. Rochon, "Reconstruction and analysis of a deciduous sapling using digital photographs or terrestrial-lidar technology," *Annals of botany*, vol. 108, no. 6, pp. 991–1000, 2011.

[27] L. Huo and X. Zhang, "A new method of equiangular sectorial voxelization of single-scan terrestrial laser scanning data and its applications in forest defoliation estimation," *Isprs journal of photogrammetry and remote sensing*, vol. 151, pp. 302–312, 2019.

[28] H. Qin, W. Zhou, Y. Yao, and W. Wang, "Individual tree segmentation and tree species classification in subtropical broadleaf forests using uav-based lidar, hyperspectral, and ultrahigh-resolution rgb data," *Remote Sensing of Environment*, vol. 280, p. 113143, 2022.

[29] M. Dassot, T. Constant, and M. Fournier, "The use of terrestrial lidar technology in forest science: application fields, benefits and challenges," *Annals of forest science*, vol. 68, pp. 959–974, 2011.

[30] M. J. Sumnall, A. Trlica, D. R. Carter, R. L. Cook, M. L. Schulte, O. C. Campoe, R. A. Rubilar, R. H. Wynne, and V. A. Thomas, "Estimating the overstory and understory vertical extents and their leaf area index in intensively managed loblolly pine (pinus taeda l.) plantations using airborne laser scanning," *Remote Sensing of Environment*, vol. 254, p. 112250, 2021.

[31] S. V. Ollinger, "Sources of variability in canopy reflectance and the convergent properties of plants," *New Phytologist*, vol. 189, no. 2, pp. 375–394, 2011.

[32] M. Öllinger, G. Jones, and G. Knoblich, "Investigating the effect of mental set on insight problem solving," *Experimental psychology*, vol. 55, no. 4, pp. 269–282, 2008.

[33] D. Baldocchi, "Measuring and modelling carbon dioxide and water vapour exchange over a temperate broad-leaved forest during the 1995 summer drought," *Plant, Cell & Environment*, vol. 20, no. 9, pp. 1108–1122, 1997.

[34] Y. Wang and P. Jarvis, "Influence of crown structural properties on par absorption, photosynthesis, and transpiration in sitka spruce: application of a model (maestro)," *Tree physiology*, vol. 7, no. 1-2-3-4, pp. 297–316, 1990.

[35] M. Béland, J.-L. Widlowski, and R. A. Fournier, "A model for deriving voxel-level tree leaf area density estimates from ground-based lidar," *Environmental Modelling & Software*, vol. 51, pp. 184–189, 2014.

[36] M. Béland and H. Kobayashi, "Mapping forest leaf area density from multiview terrestrial lidar," *Methods in Ecology and Evolution*, vol. 12, no. 4, pp. 619–633, 2021.

[37] P. Lewis, "Three-dimensional plant modelling for remote sensing simulation studies using the botanical plant modelling system," *Agronomie*, vol. 19, no. 3-4, pp. 185–210, 1999.

[38] K. Calders, J. Adams, J. Armston, H. Bartholomeus, S. Bauwens, L. P. Bentley, J. Chave, F. M. Danson, M. Demol, M. Disney *et al.*, "Terrestrial laser scanning in forest ecology: Expanding the horizon," *Remote Sensing of Environment*, vol. 251, p. 112102, 2020.

[39] J. Liu, T. Wang, A. K. Skidmore, S. Jones, M. Heurich, B. Beudert, and J. Premier, "Comparison of terrestrial lidar and digital hemispherical photography for estimating leaf angle distribution in european broadleaf beech forests," *ISPRS Journal of Photogrammetry and Remote Sensing*, vol. 158, pp. 76–89, 2019.

[40] M. Soma, F. Pimont, and J.-L. Dupuy, "Sensitivity of voxel-based estimations of leaf area density with terrestrial lidar to vegetation structure and sampling limitations: A simulation experiment," *Remote Sensing of Environment*, vol. 257, p. 112354, 2021.

[41] E. Rödig, N. Knapp, R. Fischer, F. J. Bohn, R. Dubayah, H. Tang, and A. Huth, "From small-scale forest structure to amazon-wide carbon estimates," *Nature communications*, vol. 10, no. 1, p. 5088, 2019.

[42] G. Ceccherini, M. Girardello, P. S. Beck, M. Migliavacca, G. Duveiller, G. Dubois, V. Avitabile, L. Battistella, J. I. Barredo, and A. Cescatti, "Spaceborne lidar reveals the effectiveness of european protected areas in conserving forest height and vertical structure," *Communications Earth & Environment*, vol. 4, no. 1, p. 97, 2023.

[43] M. Beland, G. Parker, B. Sparrow, D. Harding, L. Chasmer, S. Phinn, A. Antonarakis, and A. Strahler, "On promoting the use of lidar systems in forest ecosystem research," *Forest Ecology and Management*, vol. 450, p. 117484, 2019.

[44] Z. Hui, S. Jin, Y. Xia, L. Wang, Y. Y. Ziggah, and P. Cheng, "Wood and leaf separation from terrestrial lidar point clouds based on mode points evolution," *ISPRS Journal of Photogrammetry and Remote Sensing*, vol. 178, pp. 219–239, 2021.

[45] G. Zheng and L. M. Moskal, "Leaf orientation retrieval from terrestrial laser scanning (tls) data," *IEEE Transactions on Geoscience and Remote Sensing*, vol. 50, no. 10, pp. 3970–3979, 2012.

[46] F. Hosoi and K. Omasa, "Voxel-based 3-d modeling of individual trees for estimating leaf area density using high-resolution portable scanning lidar," *IEEE transactions on geoscience and remote sensing*, vol. 44, no. 12, pp. 3610–3618, 2006.

[47] M. V. N. d'Oliveira, E. O. Figueiredo, D. R. A. de Almeida, L. C. Oliveira, C. A. Silva, B. W. Nelson, R. M. da Cunha, D. de Almeida Papa, S. C. Stark, and R. Valbuena, "Impacts of selective logging on amazon forest canopy structure and biomass with a lidar and photogrammetric survey sequence," *Forest Ecology and Management*, vol. 500, p. 119648, 2021.

[48] R. Hu, E. Bournez, S. Cheng, H. Jiang, F. Nerry, T. Landes, M. Saudreau, P. Kastendeuch, G. Najjar, J. Colin *et al.*, "Estimating the leaf area of an individual tree in urban areas using terrestrial laser scanner and path length distribution model," *ISPRS journal of photogrammetry and remote sensing*, vol. 144, pp. 357–368, 2018.

[49] J. Armston, M. Disney, P. Lewis, P. Scarth, S. Phinn, R. Lucas, P. Bunting, and N. Goodwin, "Direct retrieval of canopy gap probability using airborne waveform lidar," *Remote Sensing of Environment*, vol. 134, pp. 24–38, 2013.

[50] B. N. Bailey and M. H. Ochoa, "Semi-direct tree reconstruction using terrestrial lidar point cloud data," *Remote Sensing of Environment*, vol. 208, pp. 133–144, 2018.

[51] M. P. Ferreira, J.-B. Féret, E. Grau, J.-P. Gastellu-Etchegorry, C. H. Do Amaral, Y. E. Shimabukuro, and C. R. de Souza Filho, "Retrieving structural and chemical properties of individual tree crowns in a highly diverse tropical forest with 3d radiative transfer modeling and imaging spectroscopy," *Remote Sensing of Environment*, vol. 211, pp. 276–291, 2018.

[52] S. Tao, Q. Guo, S. Xu, Y. Su, Y. Li, and F. Wu, "A geometric method for wood-leaf separation using terrestrial and simulated lidar data," *Photogrammetric Engineering & Remote Sensing*, vol. 81, no. 10, pp. 767–776, 2015.

[53] H. Shi, J. Jiang, S. Jacquemoud, Z. Xiao, and M. Ma, "Estimating leaf mass per area with leaf radiative transfer model," *Remote Sensing of Environment*, vol. 286, p. 113444, 2023.

[54] H. You, S. Li, L. Ma, and D. Wang, "Leaf area index retrieval for broadleaf trees by envelope fitting method using terrestrial laser scanning data," *IEEE Geoscience and Remote Sensing Letters*, vol. 19, pp. 1–5, 2022.

[55] L. Terryn, K. Calders, H. Bartholomeus, R. E. Bartolo, B. Brede, B. D'hont, M. Disney, M. Herold, A. Lau, A. Shenkin *et al.*, "Quantifying tropical forest structure through terrestrial and uav laser scanning fusion in australian rainforests," *Remote Sensing of Environment*, vol. 271, p. 112912, 2022.

[56] F. J. Fischer, N. Labriere, G. Vincent, B. Herault, A. Alonso, H. Memiaghe, P. Bissiengou, D. Kenfack, S. Saatchi, and J. Chave, "A simulation method to infer tree allometry and forest structure from airborne laser scanning and forest inventories," *Remote Sensing of Environment*, vol. 251, p. 112056, 2020.

[57] K. Zhou, L. Cao, H. Liu, Z. Zhang, G. Wang, and F. Cao, "Estimation of volume resources for planted forests using an advanced lidar and hyperspectral remote sensing," *Resources, Conservation and Recycling*, vol. 185, p. 106485, 2022.

[58] L. N. Guangpeng Fan, "Adqsm:a new method for estimating above-ground biomass from tls point clouds," 2020. [Online]. Available: https://github.com/GuangpengFan/AdQSM

[59] G. Fan, R. Wang, C. Wang, J. Zhou, B. Zhang, Z. Xin, and H. Xiao, "Tlsleaf: Unsupervised instance segmentation of broadleaf leaf count and area from tls point clouds," *IEEE Transactions on Geoscience and Remote Sensing*, vol. 63, pp. 1–15, 2025.

[60] L. Lu and W. J. Shuttleworth, "Incorporating ndvi-derived lai into the climate version of rams and its impact on regional climate," *Journal of Hydrometeorology*, vol. 3, no. 3, pp. 347–362, 2002.

[61] "Faro® scene software." [Online]. Available: https://www.faro.com/en/Products/Software/SCENE-Software

[62] "Speedtree." [Online]. Available: https://store.speedtree.com/

[63] L. Winiwarter, A. M. Esmorís Pena, H. Weiser, K. Anders, J. Martínez Sánchez, M. Searle, and B. Höfle, "Virtual laser scanning with helios++: A novel take on ray tracing-based simulation of topographic full-waveform 3d laser scanning," *Remote Sensing of Environment*, vol. 269, 2022.

[64] G. Fan, L. Nan, Y. Dong, X. Su, and F. Chen, "Adqsm: A new method for estimating above-ground biomass from tls point clouds," *Remote Sensing*, vol. 12, no. 18, p. 3089, 2020.

[65] Q. Wang, Y. Pang, D. Chen, X. Liang, and J. Lu, "Lidar biomass index: A novel solution for tree-level biomass estimation using 3d crown information," *Forest Ecology and Management*, vol. 499, p. 119542, 2021.

[66] M. Poorazimy, S. Shataee, R. E. McRoberts, and J. Mohammadi, "Integrating airborne laser scanning data, space-borne radar data and digital aerial imagery to estimate aboveground carbon stock in hyrcanian forests, iran," *Remote Sensing of Environment*, vol. 240, p. 111669, 2020.

[67] J. Zhao, D. Liu, Y. Cao, L. Zhang, H. Peng, K. Wang, H. Xie, and C. Wang, "An integrated remote sensing and model approach for assessing forest carbon fluxes in china," *Science of the Total Environment*, vol. 811, p. 152480, 2022.

[68] A. Bornand, N. Rehush, F. Morsdorf, E. Thürig, and M. Abegg, "Individual tree volume estimation with terrestrial laser scanning: Evaluating reconstructive and allometric approaches," *Agricultural and Forest Meteorology*, vol. 341, p. 109654, 2023.

[69] Y. Lin and J. Hyyppä, "Towards 3d basic theories of plant forms," Communications Biology, vol. 5, no. 1, p. 703, 2022.